

Hydrographic Laser Fluorosensing: Status and Perspectives

R. Reuter, R. Willkomm, O. Zielinski, W. Milchers

University of Oldenburg, Physics Department, D-26111 Oldenburg, Germany*

ABSTRACT

In 1991 a Dornier DO 228-212 aircraft was put into operation by the German Ministry of Transport for maritime surveillance of the German responsibility areas in the North Sea and the Baltic Sea. The aircraft is equipped with a Side-Looking Airborne Radar and a UV/IR scanner for the detection of oil spills. For a more detailed analysis of spills, two new instruments, a Microwave Radiometer and a Laser Fluorosensor, were integrated in 1993.

An overview on the specifications of the Laser Fluorosensor is given. It is the first instrument of its kind which meets the operational requirements for long-term use on board an aircraft. By using a conical scanner, it allows two-dimensional mapping of the sea surface in the nadir range, with 150 m swath width from 300 m aircraft altitude. Maps of oil film thickness and substance classes are derived as part of the pollution control operation.

For hydrographic application the sensor is used to measure the concentration of gelbstoff and algae by their fluorescence, and the attenuation by the water Raman signal. Kriging interpolation between flight tracks is used to derive maps of these parameters.

Based on the experience with the airborne instrument the feasibility of fluorescence measurements from space using platforms at altitudes of up to 800 km is studied. A cloudless horizontally stratified atmosphere is taken into consideration, including aerosols and ozone. A simulation based on Fermat's principle is used to describe the radiative transfer. Results are presented, such as optimised lidar parameters and an estimate of the effect of dispersion.

INTRODUCTION

In 1985 two Dornier DO 28 D2 aircraft were procured for maritime surveillance by German governmental authorities. These aircraft were equipped with side-looking airborne radar (SLAR) for detecting oil slicks over large distances, a UV/IR scanner for mapping the sea surface in the nadir-range, and TV and photcameras.

In the second generation of the German maritime surveillance system, the mission equipment has been completed by a microwave radiometer (MWR) and a laser fluorosensor (LFS). The new mapping sensors allow for a wider analysis of oil spills in terms of film thickness, and hence discharged volume. LFS data also contain information on the type of spilled substance. Moreover, some hydrographic and biological data can be measured, such as

* www.physik.uni-oldenburg.de/Docs/las/

seawater turbidity and concentrations of phytoplankton and gelbstoff which are useful parameters for estimating ecological conditions in coastal waters. A Dornier DO 228-212 aircraft allows for a flight time of up to 6 hours. An overview of this second generation surveillance system in an early stage of its realisation is given by Grüner et al. [6].

The hydrographic fluorescence lidar is described extensively in the literature, see, for example, the review by Measures [13]. Signals from natural organic compounds in seawater, like gelbstoff and phytoplankton pigments, generally interfere with the fluorescence emission of oils and need consideration when interpreting the data. The measurement of these naturally occurring substances is described in several papers [2, 4, 5, 7, 14].

Layout and specifications of the LFS developed at the University of Oldenburg and examples of two-dimensional images from oil slicks are described in Reuter et al. [15]. The application of the sensor for mapping hydrographic features, the kriging algorithm for interpolation between flight tracks, and - based on the experience with the operational airborne system - some aspects of a combined hydrographic/atmospheric lidar in space are presented here.

1. THE LASER FLUOROSENSOR

The LFS is an airborne fluorescence lidar for analysing the upper layers of the sea from aircraft flight altitudes of 100 to 300 m. It consists of

- an XeCl excimer laser for the analysis of oils, gelbstoff and organic pollutants,
- an excimer laser-pumped dye laser for chlorophyll fluorescence excitation, and hence for the measurement of phytoplankton distributions,
- a telescope with 20 cm entrance aperture, and a 12-channel spectrograph,
- a conical scanner for two-dimensional mapping of the sea-surface,
- and a VME-Bus computer for instrument control and on-line data analysis.

Since November 1993 the LFS has been operated as a component of the sensor package in a maritime surveillance aircraft. The prototype has been checked in mechanical, electronic and climatic endurance tests (crash calculations, eye safety of the laser at the operational altitude, qualification of the gas reservoir) and is now certified for permanent aircraft use.

Table 1: Laser Fluorosensor specifications

| Operating properties | |
|-----------------------------|---|
| size (l x w x h) | 1,270 x 355 x 978 mm ³ laser unit 961 x 460 x 944 mm ³ detector unit |
| weight | 315 kg |
| flight height | 1,000 ft typ. |
| electrical power | 1.0 kVA/3.4 kVA standby/at 110 Hz pulse rate |

| | | |
|---------------------------|---------------------|--------------------------|
| Lasers | XeCl excimer | dye: polyphenyl 2 |
| emission wavelength | 308 nm | 382 nm |
| pulse energy/pulse length | 150 mJ/20 ns | 20 mJ/15 ns |
| beam divergence | 2 x 10 mrad | 3 mrad |
| rep. rate peak/average | 220 Hz/110 Hz | 20 Hz/20 Hz |

Table 1: Laser Fluorosensor specifications (continued)

| | |
|-------------------------|--|
| Telescope | Cassegrain |
| entrance aperture | 20 cm |
| f-number | f/10 |
| Scanner | conical type, 20 Hz max. scan frequency, selectable |
| full scan angle | 28° across-flight, 35° in-flight |
| swath width | 150 m at 300 m flight altitude |
| pixel-to-pixel distance | 10 m typ. at 300 m flight height, 110 Hz average rep. rate |
| Spectrograph | |
| detection channels | 12 discrete, modular, optical bandwidth 10 nm typ. |
| detection wavelengths | 332, 344, 365, 382, 407, 441, 471, 492, 551, 592, 650, 684 nm |
| wavelength selection | dichroic beam splitters, glass blocking and interference filters |
| detectors | compact head-on PMT, range gated |
| A/D conversion | 12-channel gated integrator, 11 bit resolution |

2. MEASUREMENTS FROM BOARD AN AIRCRAFT

2.1. Data acquisition and processing

The fluorescence signals from gelbstoff and algae are normalised to the Raman signal for compensation of attenuation effects. Calibration of the sensor against laboratory measurements leads to absolute concentrations. The attenuation coefficient can be estimated from the inverse Raman scattered signal, if the data are compensated for geometrical (i.e. flight altitude, geometry of the scan) and sea state effects at the air-water interface.

The background signal from daylight can be a problem, when intense sun glitter directly reaches the detector or when the fluorescence signals are very weak. For routine operation algorithms have been derived to recognise faulty data and exclude them from further processing steps. Problems with sun glitter are minimised by selecting footprints of the scan pattern lying in the opposite direction compared with the azimuth of the sun. The signal-to-background ratio can be further improved by selecting lower flight altitudes.

2.2. Geostatistical interpolation of data

In oceanographic applications the use of a scanner installed on board a low flying aircraft is not meaningful, because of the much larger geometric structures in comparison to oil spills. For this purpose it is necessary to measure along several distant tracks over the area of interest. The data found along these tracks are interpolated over the whole area using geostatistical methods (Schulz-Ohlberg [16]). The advantage of these methods is the use of statistical information contained in the data.

Assuming the same statistical behaviour of the data over the whole area, the variogram

$$\gamma(h) = \frac{1}{2 N(h)} \sum_{N(h)} [Z(x+h) - Z(x)]^2 \quad (1)$$

can be derived. The correlation of data between points is statistically described as a function of their distance h , where $N(h)$ is the frequency of points with distance h and can be interpreted as a statistical distance of measured data between spatial distant points. Using this information and the kriging method the distribution of a parameter is estimated with a minimal uncertainty as a linear combination of measured values. The minimised variance is given for the whole area. This information is used to establish an optimised pattern of flight tracks. The distribution estimated with kriging shows little fluctuations because of the mean value characteristic of the interpolated data. As an advantage, large-scale structures become more obvious.

2.3. Experimental Results

Flights with the LFS operating in the hydrographic mode have been performed in the region of the Canary Islands and over the coastal waters of Germany, i.e. the German Bight and the Western Baltic. The algorithms for automatic selecting of footprints and filtering during data processing have been proved to provide reliable results. An on-line test of the data quality during measurements is important to ensure the operation of the sensor with an optimal setup under changing conditions, mainly change of water type.

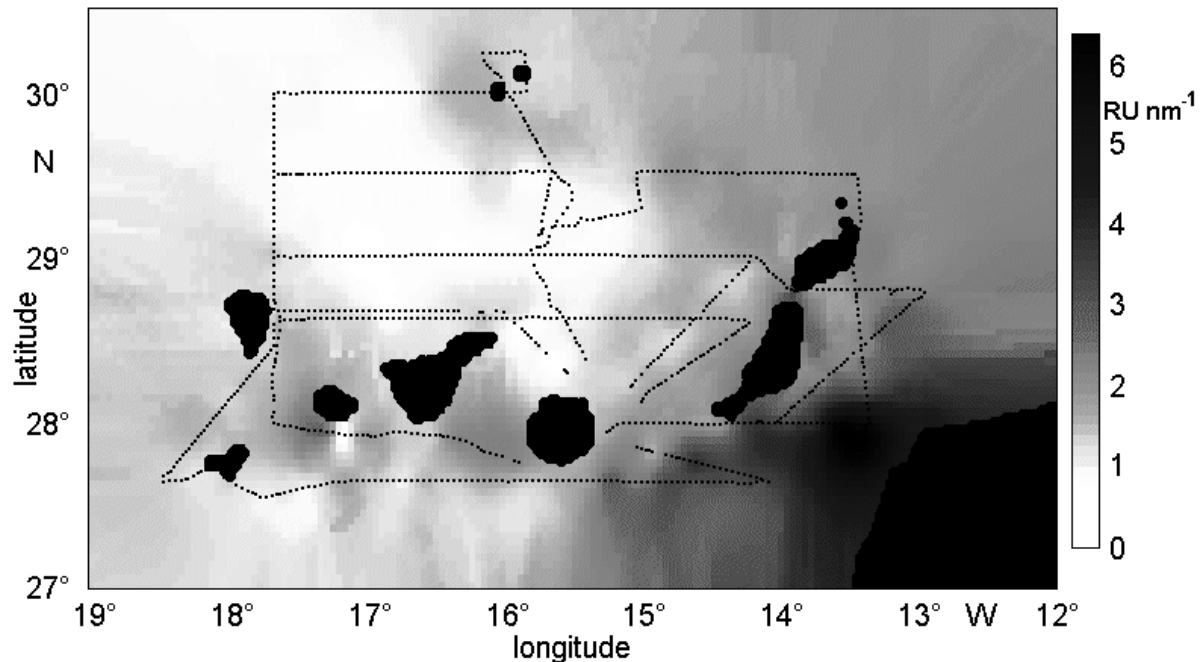


Fig. 1: Mapping of the near-surface gelbstoff distribution in the Canary Islands region, June 1995. Dotted lines show the flight tracks of four missions. Gelbstoff fluorescence was measured at 441 nm and normalised to the area of the 344 nm water Raman band as a quantitative measure of the fluorescence intensity. This signal, denoted as Raman units RU [3] is in the order of $2 \cdot 10^{-3}$ /nm at 308 nm excitation wavelength. Data measured along the flight tracks of three missions shown as dotted lines are used to derive a two-dimensional distribution with kriging. The algorithm also provides a map of estimation errors which are zero on the flight tracks and increase at more distant points (not shown here).

Under hydrographic conditions which are found in the German coastal areas the sensor is operated at 300 m altitude, providing data of the attenuation coefficient and of gelbstoff and phytoplankton chlorophyll concentrations. Measurements under daylight conditions have also been performed over waters with open ocean conditions such as the region of the Canary Islands where gelbstoff fluorescence is low. Chlorophyll concentrations of about 0.5 mg/m^3 can only be measured at nighttime because of the high daylight background.

3. MEASUREMENTS FROM SPACE

It has been shown that airborne laser remote sensing of hydrographic conditions is carried out routinely in coastal zones. However, a global monitoring programme (e.g. the Earth Observing System EOS) calls for a long-term and large-scale investigation of oceanographic processes. Some of these measurements could be achieved by a hydrographic lidar in space and it will be the object of this chapter to present the simulation of such a system, solutions to some specific problems and to outline the potential of a combined hydrographic/atmospheric lidar.

3.1. Radiative transfer in the atmosphere

Possible space platforms for a hydrographic lidar are satellites on lower earth orbits between 300 and 800 km above sea level. From these altitudes the laser beam and the detected fluorescence of a possible lidar are subject to atmospheric influences that weaken and deflect the signal. The solar induced background signal depends strongly on actual weather conditions and the angle between sun and detector. The signal-to-background ratio is essential for information retrieval. Sources of atmospheric influences for the optical information in the visible and near ultra-violet region are Rayleigh scattering (with its typical λ^{-4} dependence), absorption by ozone (O_3) - especially below 320 nm this factor is considerably higher than attenuation by tropospheric and stratospheric aerosols.

In addition to these well-known effects [1, 9, 10, 11], two factors should be examined for a complete description. A hydrographic lidar in space will change its position during the time of light propagation in the atmosphere, thus an angular correction will be necessary¹ and a beam of light started under a laser-zenith angle $\neq 0^\circ$ is deflected by the variable refraction index of air. This results in a *slant path* and by modelling the radiative transfer it will be possible to calculate the deviation and attenuation of an optical signal.

3.2. Simulation of a hydrographic lidar-in-space

In this simulation of light propagation a cloudless and horizontally stratified atmosphere is taken into consideration. The US Standard Atmosphere of 1962 with additional information on ozone and aerosols is applied [10] for the purpose of testing. The refractive index $n(z)$ at an altitude z depending on the temperature $T(z)$, the partial pressure of air $p(z)$, the partial pressure of water vapour $p_{H_2O}(z)$, and the wavelength λ are calculated using the equation by McClatchey and Selby [11]:

$$(n(z) - 1) \cdot 10^6 = \left(77.46 + \frac{0.459 \mu\text{m}^2}{\lambda^2} \right) - \frac{p(z)}{T(z)} \frac{\text{K}}{\text{hPa}} - \frac{p_{H_2O}(z)}{1013 \text{hPa}} \left(43.49 - \frac{0.347 \mu\text{m}^2}{\lambda^2} \right). \quad (2)$$

For the slant path calculation we solve Fermat's variation principle, stating that light always takes the shortest optical path, via the Euler-Lagrange differential equation. Implementing this solution in an integration over the altitude z , the deviation of a light beam of wavelength λ starting at z_1 under an angle $\Theta(z_1)$ can be calculated by

$$x(z_2) = x(z_1) + \int_{z_1}^{z_2} \frac{n(z_1)}{n(z)} \sin \Theta(z_1) \left(1 - \left(\frac{n(z_1)}{n(z)} \right)^2 \sin^2 \Theta(z_1) \right)^{-1/2} dz, \quad (3)$$

with $n(z) = n(T, p, p_{H_2O}, \lambda)$ being the refractive index of air following equation (2).

It was mentioned before that the movement of the platform during the time of light propagation calls for a small angular correction e.g. at the detector. In the first approximation one can show that a detector under an angle of

¹ For a flight altitude of 300 km the platform moves ~ 15.5 m during time elapsed between laser firing and signal return. In consequence the centres of the laser illuminated region and the detector field of view also are at a distance of ~ 15.5 m. Assuming circular patterns and a 0.6 mrad divergence for both components this leads to an overlap of only 89% of the possible maximum. A small angle correction of 0.0029° at the detector for a nadir-looking laser would compensate this movement and allow for a 100% overlap.

$$\sin \Theta_{\text{det}} = \left(x_{\text{det}} - x_{\text{probe}} \right) / \int_{z_{\text{probe}}}^{z_{\text{laser}}} \frac{n(z_{\text{probe}})}{n(z)} dz, \quad (4)$$

will correct the platform movement, if x_{probe} is the centre of the laser illuminated area calculated via Eq. (3) and x_{det} is approximated by $x_{\text{det}} \approx 2 t v_{\text{sat}}$, with t being the time the laser pulse takes from the platform to the sea surface.

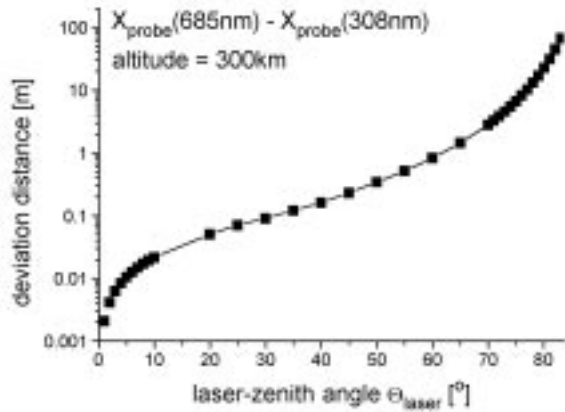


Fig. 2. Effect of dispersion of a laser beam with a variable laser-zenith-angle measured via the deviation distance for two wavelengths.

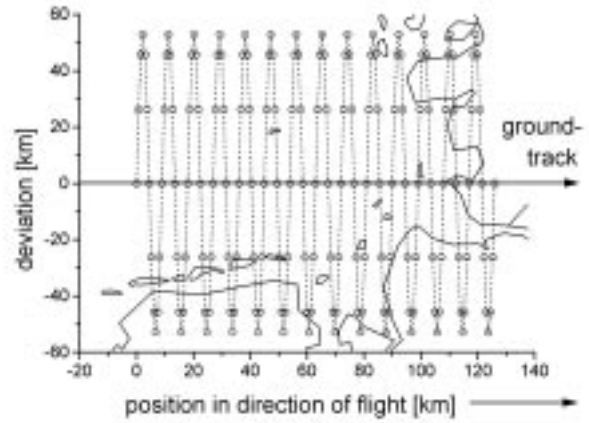


Fig. 3. Example of a scan pattern (altitude 300 km, λ 355 nm, pulse rep. rate 10 Hz, max. scan angle 10°).

Calculating the deviation of a light beam following eq. (3) for a different wavelength λ it is possible to estimate the effect of dispersion at a given laser-zenith angle Θ_{laser} . Figure 2 shows the difference of these deviations x_{probe} at 685 and 308 nm. One can see that the wavelength dependence of the refraction index can be practically neglected for $\Theta_{\text{laser}} < 60^\circ$. It is possible to calculate complete scan patterns of a hydrographic lidar using the given equations, for reasons of optimisation and illustration. Fig. 3 shows such a scan pattern for an altitude of 300 km in the German Bight, Fig. 4 summarises some proposed features of the instrument.

3.3. Layout of a spaceborne lidar

A possible laser source is a frequency tripled Nd:YAG-laser ($\lambda=355$ nm) using the absorption gap of ozone between 350 and 450 nm. Matvienko et al. [8] proposed the 1064 nm emission for simultaneous retrieval of atmospheric information. In fact the use of Nd:YAG-laser frequencies is well known from atmospheric campaigns like the Lidar In-Space Technology Experiment (LITE) [12]. A combined oceanic/atmospheric lidar offers the possibility to combine oceanographic measurements with actual atmospheric corrections, yielding quantitative concentrations of fluorescent matter in the surface layer of the ocean.

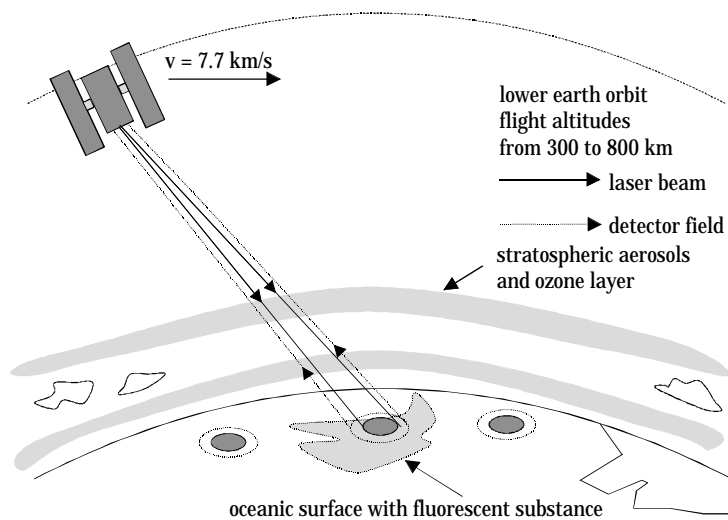


Fig. 4. Illustration of a hydrographic lidar in space

Table 2:
Proposed specifications of a hydrographic lidar in space

laser

laser type
diode pumped Nd:YAG-laser

emission wavelength
1064, 532, 355 nm

pulse repetition rate 10 Hz

beam divergence 0.3 mrad

platform

flight altitude 300 800 km

footprint distance 740 770 m

footprint diameter 90 240 m

4. DISCUSSION

As a result of the LFS development an instrument is available which is qualified for permanent installation on board an aircraft and meets the operational specifications for long-term use in maritime surveillance. When compared with nadir-looking lidars utilised earlier, the use of a scanner and a laser with high pulse firing rate yields two-dimensional maps of the sea surface, which provide a powerful tool when analysing oil spills and other structures on the ground with comparatively small geometric scales.

The experimental results described in this paper demonstrate the performance of the LFS and its capability of mapping medium-scale hydrographic features. The area covered by one flight with the Dornier DO 228 aircraft is about $50,000 \text{ km}^2$. Pollution control flights performed over German coastal areas on a regular basis give the opportunity of monitoring the change of hydrographic parameters in time scales of one week.

Additionally we have stated that a spaceborne hydrographic lidar holds the possibility of long-term and large-scale monitoring of bio-optical components like yellow-substance and chlorophyll. The simulation of radiative transfer via a specific solution of Fermat's principle enables the optimisation of lidar angle configuration. We can also show that effects caused by dispersion in the atmosphere can be neglected at small laser-zenith angles. For an improved correction of fluorescence signals a simultaneous measurement of atmospheric parameters of a combined hydrographic/atmospheric lidar is proposed and possible specifications are given.

ACKNOWLEDGEMENTS

Development of the Laser Fluorosensor was financially supported by the DLR Project Executive Department Environmental Protection and Technologies, Bonn, on behalf of the Federal Ministry for Research and Technology. We are grateful to the staff of the Naval Air Wing 3 in Nordholz for their co-operation during hydrographic experiments.